Constraining postinflationary axions with pulsar timing arrays

Géraldine Servant[1,2,*] and Peera Simakachorn[3,†]

[1]*Deutsches Elektronen-Synchrotron DESY, Notkestrasse 85, 22607 Hamburg, Germany*
[2]*II. Institute of Theoretical Physics, Universität Hamburg, 22761 Hamburg, Germany*
[3]*Instituto de Física Corpuscular (IFIC), Universitat de València-CSIC, C/ Catedrático José Beltrán 2, E-46980 Paterna, Spain*

(Received 20 July 2023; accepted 19 October 2023; published 11 December 2023)

Models that produce axionlike particles (ALPs) after cosmological inflation due to spontaneous $U(1)$ symmetry breaking also produce cosmic-string networks. Those axionic strings lose energy through gravitational-wave emission during the whole cosmological history, generating a stochastic background of gravitational waves that spans many decades in frequency. We can therefore constrain the axion decay constant and axion mass from limits on the gravitational-wave spectrum and compatibility with dark matter abundance as well as dark radiation. We derive such limits from analyzing the most recent NANOGrav data from pulsar timing arrays (PTAs). The limits are similar to the $N_{\rm eff}$ bounds on dark radiation for ALP masses $m_a \lesssim 10^{-22}$ eV. On the other hand, for heavy ALPs with $m_a \gtrsim 0.1$ GeV and $N_{\rm DW} \neq 1$, new regions of parameter space can be probed by PTA data due to the dominant domain-wall contribution to the gravitational-wave background.

DOI: 10.1103/PhysRevD.108.123516

I. INTRODUCTION

Pulsar timing arrays (PTAs) offer a new window to observe the Universe through gravitational waves (GWs) in the nanohertz frequency range [1–6]. A potential source of GWs at these frequencies is a population of supermassive black hole binaries (SMBHBs) in the local Universe [6,7]. Additionally, cosmic strings, which may have been produced in the early Universe during a spontaneous $U(1)$ symmetry-breaking event [8–11], generate a stochastic gravitational-wave background (SGWB) down to these low frequencies as part of a vast spectrum spanning many decades in frequency; see Refs. [12,13] for recent reviews. In fact, given the very wide and nearly scale-invariant GW spectrum from cosmic strings, the PTA limits are very relevant to anticipate the prospects for probing a cosmic-string GW signal at the Laser Interferometer Space Antenna (LISA) [14] or Einstein Telescope [15]. Cosmic strings can either be local or global depending on whether the spontaneously broken symmetry is a gauge or global $U(1)$. Models of local strings have been confronted to PTA data in [16–19] and, most recently, to the 15-year NANOGrav (NG15) data in [5] and the EPTA data release 2 [6,20].

This paper focuses instead on GWs from global strings [12,21–25], which were not analyzed in [5]. Many Standard Model extensions feature such additional global $U(1)$ symmetry that gets spontaneously broken by the vacuum expectation value of a complex scalar field, thus delivering a Nambu-Goldstone boson. A famous example is the Peccei-Quinn $U(1)$ symmetry advocated to solve the strong CP problem and its associated axion particle [26–29]. Because the $U(1)$ symmetry gets also broken explicitly at later times, the axion acquires a mass. At that moment, domain walls can also populate the Universe [30].

This paper considers this broad class of models of so-called axionlike particles (ALPs) with mass m_a and decay constant f_a, corresponding to the energy scale of spontaneous symmetry breaking. If the cosmic-string and domain-wall formations happen before inflation, those are diluted away. On the other hand, if the $U(1)$ is broken at the end or after inflation (in this case, the ALP is dubbed "postinflationary"), cosmic strings give rise to a population of loops that generate a SGWB throughout the cosmic history. At the same time, they also generate axion particles [31–37], while domain walls bring an additional contribution to the GW spectrum [38–45].

We aim to use the most recent limits on the SGWB from NG15 dataset to derive independent bounds on the parameter space of postinflationary ALPs. Given that a GW signal has been observed [1], any further improved sensitivity from future PTA observatories will not enable pushing down the constraints. Therefore, the PTA constraints presented in this paper on the axion mass and decay constant are not expected to change by more than a factor of a few from

*geraldine.servant@desy.de
†peera.simakachorn@ific.uv.es

future PTA experiments. On the other hand, future GW experiments operating in other frequency ranges will serve as complementary probes to PTAs.

Our approach is the following. We analyze the recent NG15 data via the code PTArcade [46,47], first considering the two SGWBs from global cosmic strings and domain walls without the astrophysical background. We compare the interpretation of data in terms of SMBHBs and of global cosmic strings and domain walls by calculating the Bayes factor (BF). Next, we set constraints on the new-physics contribution, leading to a SGWB that is too strong and conflicts with the data. The results of the best fit and the constraints on the SGWB from domain walls have been presented in the recent analysis with NG15 data by the NANOGrav Collaboration [5]. Regarding the analysis of previous data releases, Refs. [48–50] fitted the domain-wall and/or global-string signal to the PPTA second data release (DR2) or IPTA DR2 and/or NANOGrav 12.5-yr data, however, did not derive the exclusion region. (See Sec. III for more details on the best fit and constraint.) We further translate these bounds into constraints in the ALP parameter space. In addition, this work presents a similar analysis (determining best fits and setting constraints) for global strings for the first time with NG15.

Section II of this paper summarizes the postinflationary axion scenarios and their corresponding GW signals, separated into two cases: either cosmic-string or domain-wall SGWB dominates. In Sec. III, we confront these cases with the NG15 data and derive, for each case, the constraints on axion parameter space, illustrated in Fig. 3. We conclude in Sec. IV.

The Appendixes contain miscellaneous details, such as the priors for analysis, the case assuming no astrophysical background, and the result for the global strings in the $m_a \to 0$ limit, as well as giving more details on analyzing NG15 data with the global-string and domain-wall templates. Appendix A specifies the priors used in this study. Appendix B discusses the possible modification of the PTA constraint from global strings in the parameter region where the axion is overabundant (even though this scenario is excluded). We then present in Appendix C the best fits without and with the astrophysical background and compare them using the Bayes factor method. Appendix D presents the results of the global-string template in the limit $T_{\rm dec} \to 0$ (or $m_a \to 0$), the so-called "stable" global strings. We also summarize, in Appendix E, the confidence levels associated with interpretations of the NG15 dataset with the GW signal discussed in this paper, compared to other cosmological backgrounds considered in [5]. Our analysis includes the temperature dependence of the number of relativistic degrees of freedom g_* and g_{*s}, taken from Ref. [51].

II. POSTINFLATIONARY AXION AND ITS GRAVITATIONAL WAVES

The ALP can be defined as the angular mode θ of a complex scalar field $\Phi \equiv \phi \exp(i\theta)$ with ϕ the radial partner. It has the Lagrangian density $\mathcal{L} = \frac{1}{2}\partial_\mu \Phi^* \partial^\mu \Phi - V(\Phi) - V_c$ with V_c the correction responsible for $U(1)$ symmetry restoration and trapping $\Phi \to 0$ at early times. The potential has three terms,

$$V(\Phi) = \underbrace{\frac{\lambda}{2}(\phi^2 - f_a^2)^2}_{\text{cosmic strings}} + \underbrace{\frac{m_a^2 f_a^2}{N_{\rm DW}^2}[1 - \cos(N_{\rm DW}\theta)]}_{\text{domain walls}} + V_{\rm bias},$$

where f_a is the vacuum expectation value of the field, $m_a \equiv m_a(T)$ is the axion mass as a function of the Universe's temperature T, $N_{\rm DW}$ is the number of domain walls, and $V_{\rm bias}$ is some further explicit $U(1)$-breaking term. The first term is responsible for $U(1)$ spontaneous breaking, while the second and third terms explicitly break the $U(1)$. These three terms are ranked according to their associated energy scales (large to small) corresponding to their sequences in defect formations: from cosmic strings to domain walls and then their decays.

During inflation, the complex scalar field is driven to the minimum of the potential $V(\Phi)$ if $V_c \ll V(\Phi)$. Quantum fluctuations along the axion direction due to the de Sitter temperature $\mathcal{O}(H_{\rm inf})$ can generate a positive quadratic term in the potential and restore the $U(1)$ symmetry, which gets eventually broken at the end of inflation, leading to cosmic strings if $H_{\rm inf}/(2\pi f_a) \gtrsim 1$ [52–54]. However, the current cosmic microwave background (CMB) bound [55] on the inflationary scale $H_{\rm inf} < 6.1 \times 10^{13}$ GeV implies that f_a is too small to generate an observable cosmic-string SGWB. Still, there are several other ways in which $U(1)$ can get broken after inflation even for large f_a: (i) A large and positive effective ϕ mass can be generated by coupling ϕ to the inflaton χ (e.g., $\mathcal{L} \supset \chi^2\phi^2$) which, for large χ, traps $\phi \to 0$ during inflation.[1] (ii) ϕ could couple to a thermal (Standard Model or secluded) plasma of temperature T that would generate a large thermal V_c correction, restoring the $U(1)$.[2] (iii) Finally, nonperturbative processes, such as preheating, could also lead to $U(1)$ restoration after inflation [58–62].

When V_c drops, the first term of $V(\Phi)$ breaks spontaneously the $U(1)$ symmetry at energy scale f_a, leading to the network formation of linelike defects or "cosmic

[1]As the inflaton field value relates to the Hubble parameter, this mass is called "Hubble-induced" mass.

[2]For example, the Kim-Shifman-Vainshtein-Zakharov- (KSVZ) type of interaction couples ϕ to a fermion ψ charged under some gauge symmetry with A_μ: $\mathcal{L} \supset y\phi\bar{\psi}\psi + \text{H.c.} + g\bar{\psi}\gamma^\mu\psi A_\mu$, which can generate thermal corrections: $V_c = y^2T^2\phi^2$ for $y\phi < T$ and $V_c = g^4T^4\ln(y^2\phi^2/T^2)$ for $y\phi \gtrsim T$ [56,57]. When $V_c > \lambda f_a^4$, the ϕ field is trapped at the origin at temperature $T \gtrsim \sqrt{\lambda} f_a/y$ for $yf_a < T$ and $T \gtrsim \lambda^{1/4} f_a/g$ for $yf_a > T$. For couplings of order unity, $f_a < T < T_{\rm max} \simeq 6.57 \times 10^{15}$ GeV is the maximum reheating temperature bounded by the inflationary scale and assuming instantaneous reheating. Nonetheless, if λ is small (corresponding to a small radial-mode mass), the bound can be weakened.

strings" with tension $\mu = \pi f_a^2 \log(\lambda^{1/2} f_a/H)$ [11]. As $U(1)$ symmetry is approximately conserved when the axion mass is negligible, the cosmic strings survive for long and evolve into the "scaling regime" by chopping off loops [63–76]. Loops are continuously produced and emit GWs and axion particles throughout cosmic history. The resulting GW signal corresponds to a SGWB entirely characterized by its frequency power spectrum. The latter is commonly expressed as the GW fraction of the total energy density of the Universe $h^2\Omega_{\rm GW}(f_{\rm GW})$.

A loop population produced at temperature T quickly decays into GWs of frequency [12],

$$f_{\rm GW}^{\rm CS}(T) \simeq 63\ {\rm nHz}\left(\frac{\alpha}{0.1}\right)\left(\frac{T}{10\ {\rm MeV}}\right)\left[\frac{g_*(T)}{10.75}\right]^{\frac{1}{4}}, \quad (1)$$

where $\alpha \sim \mathcal{O}(0.1)$ is the typical loop size in units of the Hubble horizon $1/H$. If the network of cosmic strings is stable until late times, i.e., in the limit $m_a \to 0$, its SGWB is characterized by [12,77]

$$h^2\Omega_{\rm GW}^{\rm CS}(f_{\rm GW}) \simeq 1.3\times 10^{-9}\left(\frac{f_a}{3\times 10^{15}\ {\rm GeV}}\right)^4 \times \mathcal{G}(T(f_{\rm GW}))\left[\frac{\mathcal{D}(f_a, f_{\rm GW})}{94.9}\right]^3\left[\frac{C_{\rm eff}(f_{\rm GW})}{2.24}\right], \quad (2)$$

where $\mathcal{G}(T) \equiv [g_*(T)/g_*(T_0)][g_{*s}(T_0)/g_{*s}(T)]^{4/3}$ with T_0 the temperature of the Universe today. The logarithmic correction is defined by

$$\mathcal{D}(f_a, f_{\rm GW}) = \log\left[1.7\times 10^{41}\left(\frac{f_a}{3\times 10^{15}\,{\rm GeV}}\right)\left(\frac{10\,{\rm nHz}}{f_{\rm GW}}\right)^2\right], \quad (3)$$

and $C_{\rm eff}(f_{\rm GW})$ is the loop-production efficiency that also receives a small log correction originating from axion production [12]. g_* and g_{*s} measure the number of relativistic degrees of freedom in the energy and entropy densities, respectively. Note that the exponent "3" of the log-dependent term $\mathcal{D}$ is still under debate [23,35–37,78–85]. For example, some numerical simulations find the scaling network leading to the exponent 3 [85], while the nonscaling one leads to the exponent "4" [23,35,36]. From Eq. (2), the uncertainty in $\Omega_{\rm GW}$ due to a factor of $\mathcal{D} \sim \mathcal{O}(100)$ leads to the uncertainty in the constraint on f_a by $\sim 10^{1/2}$. Moreover, the recent debate on the GW-emission power from a single loop in different numerical simulations is open [23,86]. This work uses the semianalytic result, e.g., in [12,21,22], which predicts $\Omega_{\rm GW}$ that is weaker than [23] and stronger than [86].

As the Universe cools, the axion mass develops due to nonperturbative effects (like strong confinement in the case of the QCD axion). The second term in $V(\Phi)$ breaks explicitly the $U(1)$ discretely, leading to sheetlike defects or "domain walls," attached to the cosmic strings. The domain wall is characterized by its surface tension $\sigma \simeq 8 m_a f_a^2/N_{\rm DW}^2$ [42]. The axion field starts to feel the presence of the walls when $3H \simeq m_a$. The domain-wall network can be stable or unstable depending on the number of domain walls attached to a string. The value of $N_{\rm DW}$ is very UV-model dependent. It can be linked to the discrete symmetry $Z_{N_{\rm DW}}$ [87–89] that remains after the confinement of the gauge group that breaks the global $U(1)$ symmetry explicitly and generates the axion mass. This occurs at the scale $\Lambda \simeq \sqrt{m_a F_a}$, where $F_a = f_a/N_{\rm DW}$; that is, when the domain walls (DWs) are generated, attaching to the existing cosmic strings.

For $N_{\rm DW} > 1$, the string-wall system is stable and long-lived. Its decay may be induced by $V_{\rm bias}$, the biased term [90–92], which could be of QCD origin [30,40]. This decay is desirable to prevent DWs from dominating the energy density of the Universe at late times. $V_{\rm bias}$ is therefore an additional free parameter beyond m_a and f_a that enters the GW prediction in the case where $N_{\rm DW} > 1$.

A. Case (i) $N_{\rm DW} = 1$

If only one domain wall is attached to a string, i.e., $N_{\rm DW} = 1$, the string-wall system quickly annihilates due to DW tension when[3] $H(T_{\rm dec}) \simeq m_a$ [41]. The cosmic-string SGWB features an IR cutoff corresponding to the temperature

$$T_{\rm dec} \simeq 1.6\ {\rm MeV}\left[\frac{10.75}{g_*(T_{\rm dec})}\right]^{\frac{1}{4}}\left(\frac{m_a}{10^{-15}\ {\rm eV}}\right)^{\frac{1}{2}}, \quad (4)$$

associated with the frequency

$$f_{\rm GW}^{\rm CS}(m_a) \simeq 9.4\ {\rm nHz}\left(\frac{\alpha}{0.1}\right)\left(\frac{m_a}{10^{-15}\ {\rm eV}}\right)^{\frac{1}{2}}. \quad (5)$$

The cutoff position—frequency and amplitude—can be estimated with Eqs. (2)–(5). At $f_{\rm GW} < f_{\rm GW}^{\rm CS}(T_{\rm dec})$, the spectrum scales as $\Omega_{\rm GW} \propto f_{\rm GW}^3$ due to causality. Note that, for $m_a \ll 10^{-16}$ eV, the cutoff sits below nanohertz frequencies, and within the PTA window, we recover the same GW spectrum as the one in the limit $m_a \to 0$. Our analysis applies the numerical templates of the global-string SGWB—covering the ranges of f_a and $T_{\rm dec}$ priors. We calculated these templates numerically by solving the string-network evolution via the "velocity-dependent one-scale model" [69,94–97], shutting off the loop production after $H = m_a$, and calculating the SGWB following Ref. [12].

[3]The string tension loses against the DW surface tension at time $t_{\rm dec}$ defined by [93] $F_{\rm str} \sim \mu/R_{\rm dec} \simeq \sigma \Rightarrow R_{\rm dec} \sim H^{-1}(t_{\rm dec}) \sim \mu/\sigma \sim m_a^{-1}$ where R is the string curvature, assumed to be of Hubble size.

B. Case (ii) $N_{\rm DW} > 1$

Attached to a string, $N_{\rm DW}$ walls balance among themselves and prevent the system from collapsing at $H \simeq m_a$ [41,98]. The domain-wall network later evolves to the scaling regime where there is a constant number of DW per comoving volume $\mathcal{V} \simeq H^{-3}$. The energy density of DW is $\rho_{\rm DW} \simeq \sigma H^{-2}/\mathcal{V} \simeq \sigma H$ and it acts as a long-lasting source of SGWB [90,99–104]; cf. [105] for a compact review. The network redshifts slower than the Standard Model (SM) radiation energy density and could dominate the Universe. The biased term $V_{\rm bias}$—describing the potential difference between two consecutive vacua—explicitly breaks the $U(1)$ symmetry and induces the pressure on one side of the wall [8,90]. Once this pressure overcomes the tension of the wall,[4] the string-wall system collapses at temperature

$$T_\star \simeq 53\ \text{MeV}\left[\frac{10.75}{g_*(T_*)}\right]^{\frac{1}{4}}\left[\frac{V_{\rm bias}^{\frac{1}{4}}}{10\ \text{MeV}}\right]^2\left[\frac{\text{GeV}}{m_a}\right]^{\frac{1}{2}}\left[\frac{10^6\ \text{GeV}}{f_a/N_{\rm DM}}\right]. \tag{6}$$

The fraction of energy density in the DW is maximized at this time and reads

$$\begin{aligned}\alpha_\star &\equiv \rho_{\rm DW}/\rho_{\rm tot}(T_\star) \simeq \sigma H/(3M_{\rm Pl}^2H^2(T_\star)),\\ &\simeq 4\times10^{-4}\left[\frac{10.75}{g_*(T_\star)}\right]^{\frac{1}{2}}\left[\frac{m_a}{\text{GeV}}\right]\left[\frac{f_a/N_{\rm DW}}{10^6\ \text{GeV}}\right]^2\left[\frac{50\ \text{MeV}}{T_\star}\right]^2.\end{aligned} \tag{7}$$

The energy density emitted in GWs is [42]

$$\rho_{\rm GW}/\rho_{\rm tot} \sim \frac{3}{32\pi}\epsilon\alpha_\star^2, \tag{8}$$

where we fix $\epsilon \simeq 0.7$ from numerical simulations [103]. It reaches its maximum at $T_\star$. The spectrum exhibits the broken-power-law shape and reads

$$\begin{aligned}h^2\Omega_{\rm GW}^{\rm DW}(f_{\rm GW}) \simeq 7.35\times10^{-11}&\left[\frac{\epsilon}{0.7}\right]\left[\frac{g_*(T_\star)}{10.75}\right]\left[\frac{10.75}{g_{*s}(T_\star)}\right]^{\frac{4}{3}}\\ &\times\left(\frac{\alpha_\star}{0.01}\right)^2\mathcal{S}\left(\frac{f_{\rm GW}}{f_{\rm p}^{\rm DW}}\right),\end{aligned} \tag{9}$$

where the normalized spectral shape is

$$\mathcal{S}(x) = (3+\beta)^\delta/(\beta x^{-\frac{3}{\delta}} + 3x^{\frac{\beta}{\delta}})^\delta. \tag{10}$$

The $f_{\rm GW}^3$-IR slope is dictated by causality, the UV slope $f_{\rm GW}^\beta$ is model dependent, and the width of the peak is δ.

[4]The pressure from $V_{\rm bias}$ is $p_V \sim V_{\rm bias}$, while the wall's tension reads $p_T \sim \sigma H$ assuming the wall of horizon size. The collapse happens when $p_V > p_T$.

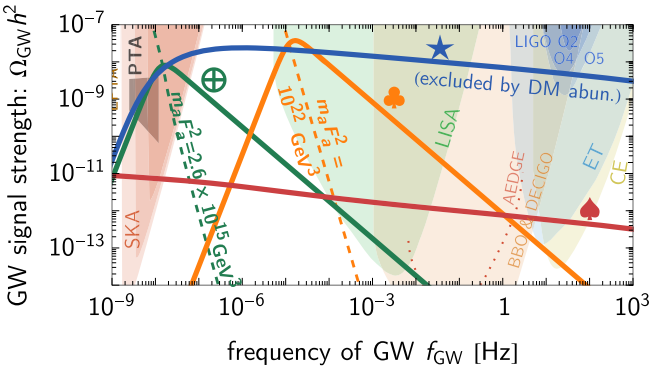

FIG. 1. Solid curves show the SGWB spectra from axionic strings for $N_{\rm DW} = 1$ {blue star, red spade} and domain walls for $N_{\rm DW} > 1$ {green circle-plus, orange club}. The symbols correspond to the benchmark points in the axion parameter space in Fig. 3 (with $T_\star = \{128\ \text{MeV}, 10^2\ \text{GeV}\}$ for {circle-plus, club}). The best-fitted spectra to the PTA data are the blue star curve for global strings, corresponding to $\{f_a, m_a\} \simeq \{9.9\times10^{15}\ \text{GeV}, 4.8\times10^{-15}\ \text{eV}\}$ which is excluded by the axion dark matter (DM) abundance [see Eq. (14)], and the green circle-plus curve for domain walls (with $m_aF_a^2 = 2.6\times10^{15}\ \text{GeV}^3$). The power-law integrated sensitivity curves of GW experiments [14,106–119] are taken from [12,120]. For fixed $\{m_a, f_a\}$ values, the peak of the DW-GW spectrum moves along the dashed line as $T_\star$ varies; see Eq. (12).

The peak frequency corresponds to the DW size, i.e., the horizon size $f_{\rm GW}^\star \sim H_\star$ [103]. Its value today reads

$$f_{\rm p}^{\rm DW} \simeq 1.14\ \text{nHz}\left[\frac{g_*(T_\star)}{10.75}\right]^{\frac{1}{2}}\left[\frac{10.75}{g_{*s}(T_\star)}\right]^{\frac{1}{3}}\left[\frac{T_\star}{10\ \text{MeV}}\right]. \tag{11}$$

From Eqs. (7), (9), and (11), each value of $m_af_a^2$ corresponds to a degenerate peak position of the GW spectrum,

$$\begin{aligned}h^2\Omega_{\rm GW}^{\rm DW}(f_{\rm p}^{\rm DW}) \simeq 1.2\times10^{-10}&\left[\frac{\epsilon}{0.7}\right]\left[\frac{g_*(T_\star)}{10.75}\right]^3\left[\frac{10.75}{g_{*s}(T_\star)}\right]^{\frac{8}{3}}\\ &\times\left[\frac{m_a}{\text{GeV}}\right]^2\left[\frac{f_a}{10^6\ \text{GeV}}\right]^4\left[\frac{\text{nHz}}{f_{\rm p}^{\rm DW}}\right]^4,\end{aligned} \tag{12}$$

which are shown as the dashed line in Fig. 1.

The DW can decay into axions, which either behave as dark radiation or decay into SM particles. When DWs decay into dark radiation, the $\Delta N_{\rm eff}$ puts a bound $\alpha_\star \lesssim 0.06$ [48], i.e., the peak of the GW spectrum has $h^2\Omega_{\rm GW} \lesssim 10^{-9}$ (which cannot fit the whole 14 bins of NG15 data). As $\alpha_\star$ controls the amplitude of the GW spectrum (9), we consider a larger range of $\alpha_\star$, up to $\alpha_\star = 1$ when the energy density of the DWs start to dominate the Universe. To get around the $\Delta N_{\rm eff}$ bound, we will therefore consider the case where the axions produced by domain walls eventually decay into SM particles.

In this paper, we confront the most recent PTA data for both cases: (i) $N_{\rm DW} = 1$, where the SGWB in the PTA

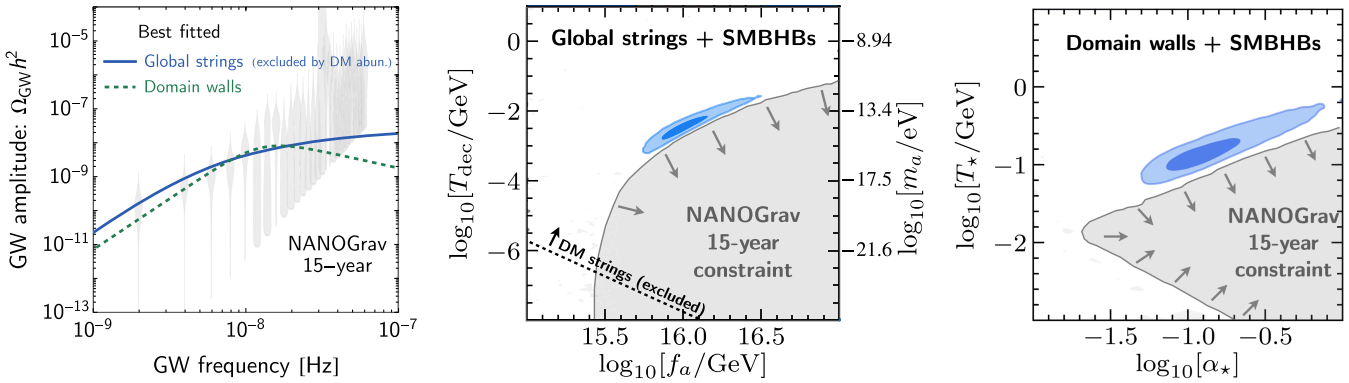

FIG. 2. Left: the SGWB spectra from global strings and domain walls + SMBHBs, providing the best fits to the PTA data and corresponding to $\{f_a, m_a\} \simeq \{9.9 \times 10^{15}\ \text{GeV}, 4.8 \times 10^{-15}\ \text{eV}\}$ for global strings and $m_a F_a^2 = 2.6 \times 10^{15}\ \text{GeV}^3$ for domain walls (in violins, taken from [5]). Middle and right: 1σ (dark blue) and 2σ (light blue) regions of the likelihood of the global-string/domain-wall parameters, assuming the template of global-string/domain-wall + SMBHB backgrounds. The gray region is excluded due to too strong GW signals from global strings/domain walls that conflict with PTA data. The region above the black dashed line in the middle panel (including the best fit) conflicts with the dark matter abundance [see Eq. (14)].

range dominantly comes from the cosmic strings, and (ii) $N_{\rm DW} > 1$, where the SGWB in the PTA range comes from the domain walls. These two cases correspond to axions of two utterly different mass ranges. For case (i), the cosmic strings live long; that is, m_a is small. Instead, case (ii) corresponds to the large m_a region. We compare the GW spectra in Fig. 1 for different benchmark points, corresponding to locations in the $\{m_a, F_a\}$ plane, which are shown in Fig. 3.

III. SEARCHING AND CONSTRAINING SGWB WITH PTAs

This work analyzes the recent NG15 dataset [121] covering a period of observation $T_{\rm obs} = 16.03$ yr [1]. From the pulsar timing residuals, the posterior probability distributions of the global-string and domain-wall model parameters are derived. We consider 14 frequency bins of NG15 data, where the first and last bins are at $1/T_{\rm obs} \simeq 1.98$ and $14/T_{\rm obs} \simeq 27.7$ nHz, respectively. The analysis is done by using ENTERPRISE [122,123] via the handy wrapper PTArcade [46,47]. The priors for the model parameters are summarized in Table I in Appendix A. We refer readers to Ref. [5] for a short review of Bayesian analysis.

This work considers the SGWB in the two scenarios discussed above together with the astrophysical background. Figure 2 (middle and right) show the 68% confidential level (CL) (or 1σ) and 95% CL (or 2σ) in dark and light blue regions, respectively. We obtain the best-fit values $f_a = 9.87^{+2.67}_{-2.02} \times 10^{15}$ GeV and $T_{\rm dec} = 3.50^{+2.44}_{-1.48}$ MeV for global strings, and $\alpha_\star = 0.114^{+0.060}_{-0.033}$ and $T_\star = 128^{+55}_{-33}$ MeV for domain walls. The global-string and domain-wall SGWB are preferred over the SMBHB signal implemented by PTArcade, as suggested by their BFs larger than unity ($\text{BF}_{\rm CS} = 26.0$, $\text{BF}_{\rm DW} = 44.7$) when compared to the SMBHB interpretation; cf. Eq. (9) of [5]. We show the best-fitted spectra for these two new-physics cases in Fig. 2 (left). Translating into axion parameters via Eqs. (4) and (7), the best fits correspond to $\{f_a, m_a\} = \{9.87 \times 10^{15}\ \text{GeV}, 4.78 \times 10^{-15}\ \text{eV}\}$ for global strings (excluded by the axion overabundance) and $m_a F_a^2 = 2.6 \times 10^{15}\ \text{GeV}^3$ for domain walls. For completeness, we show the case without the SMBHB contribution in Appendix C. Because the two new-physics cases explain the data well by themselves, we see that the 1σ and 2σ regions of Fig. 2 match those without the SMBHB in Fig. 5. The values of the best fits, given in Appendix C, only change slightly.

Although the two scenarios could explain the signal, this work aims to set bounds on the model parameter space associated with a too strong SGWB in conflict with the NG15 data. Following [5], we identify excluded regions of the new-physics parameter spaces using the posterior probability ratio (or K ratio). Specifically, the excluded gray regions in Fig. 2 (middle and right) correspond to the areas of parameter spaces where the K ratio between the combined new-physics + SMBHB and the SMBHB-only models drops below 0.1,[5] according to the Jeffreys scale [124], due to a too-strong SGWB from the new-physics model. We emphasize that the values of the BFs strongly depend on the modeling of the SMBHB signal as it is the ratio of evidence of the considered model and the SMBHB template. However, the constrained regions depend only slightly on it [5].

We emphasize that the constraints on the axion parameter space presented in this paper are not the same as the regions of best fit obtained in the literature using the previous dataset, e.g., [48,50]. For fitting the PTA data, a particular part of the GW spectrum is preferred; thus, the

[5]That is, the new-physics contribution makes the overall signal *strongly* disfavored by the data.

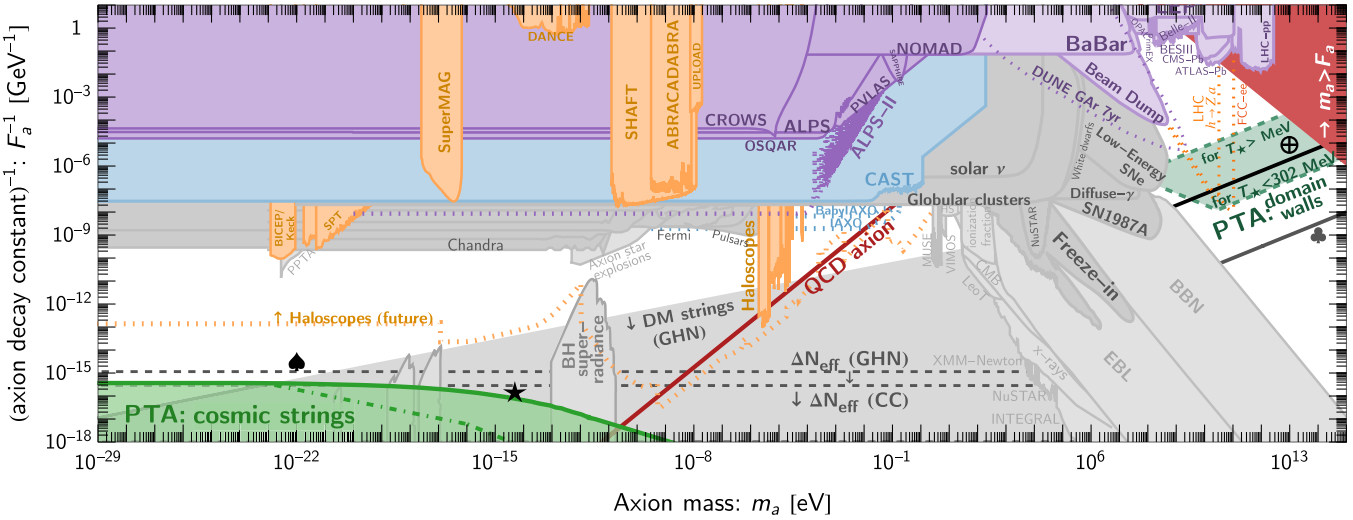

FIG. 3. PTA limits (in green) on postinflationary axions, compared to existing experimental constraints as compiled from AxionLimits [125] and to theoretical bounds: dark radiation overabundance $\Delta N_{\rm eff}$ bound (13) as dashed horizontal line and ALP overabundance (14) in the shaded gray region. $F_a = f_a/N_{\rm DW}$. The orange dotted lines in the $m_a \gtrsim 1$ GeV region are the projections of future collider experiments, LHC ($h \to Za$) and Future circular collider (FCC) ($e^+e^- \to ha$), obtained from [126,127] with the maximally allowed ALP-SM coupling. The red region denoted $m_a > F_a$ is where the axion effective field theory is not valid. The comparison with experimental bounds uses $g_{\theta\gamma\gamma} = 1.02\alpha_{\rm EM}/(2\pi F_a) \approx 2.23 \times 10^{-3}/F_a$ for the relation between the photon coupling and F_a, as motivated by KSVZ models [128,129]. The recent PTA data [1] excludes the green small-m_a region due to cosmic-string SGWB ($N_{\rm DW} = 1$). It also potentially excludes the high-m_a region due to domain-wall SGWB for $N_{\rm DW} > 1$, depending on the value of $T_\star$. The other green band at large m_a is the region that PTAs can constrain if $T_\star$ varies in the range MeV $< T_\star <$ 302 MeV, as illustrated in Fig. 4. The two benchmark points {star, spade} correspond to cosmic-string SGWB, and the two black benchmark lines {circle-plus, club} correspond to the domain-wall SGWB, whose spectra are shown in Fig. 1. The green dot-dashed line is explained in Appendix B.

best-fit region is allowed within a tight parameter space (the blue blobs in Fig. 2). On the other hand, the constraint can be drawn from any part of the spectrum if the GW signal becomes too large and disfavored by the data. So, the constraint can be extended over a vast parameter space (the gray regions in Fig. 2). Now we discuss, in turn, the NG15 constraints—on global strings ($N_{\rm DW} = 1$) and domain walls ($N_{\rm DW} > 1$)—and translate them into the constraints in the axion parameter space.

A. Result for $N_{\rm DW} = 1$, implications for light axions

We fit the PTA data with the global-string SGWB, varying $\{f_a, T_{\rm dec}\}$. The 2D posterior result is shown in Fig. 2, and the dark blue region is where the cosmic-string SGWB dominates and fits the data to the significance of 1σ with the best fit $\{f_a, m_a\} \simeq \{9.9 \times 10^{15}$ GeV, 4.8×10^{-15} eV$\}$, shown as the benchmark case star in Figs. 1 and 3. Note that this benchmark point is excluded by the axion overabundance constraint [see Eq. (14)]. A too-large global-string SGWB is constrained by PTAs in the gray region of Fig. 2 (middle). For small f_a, the GW from cosmic strings cannot fit the data as its amplitude becomes too small.

As $T_{\rm dec} \ll 0.1$ MeV ($m_a \ll 10^{-17}$ eV), the cutoff (5) associated with $T_{\rm dec}$ moves below the PTA window [$f_{\rm GW}(T_{\rm dec}) <$ nHz]. The constraint in this case, Fig. 2 (middle), reads $f_a < 2.8 \times 10^{15}$ GeV (m_a independent), which is stronger than the LIGO bound[6] ($f_a \lesssim 8 \times 10^{16}$ GeV). For completeness, we also analyzed the case of stable global strings (i.e., $m_a \to 0$) in Appendix D, and we obtained a similar bound. For $T_{\rm dec} \gg 0.1$ MeV ($m_a \gg 10^{-17}$ eV), the cutoff sits at a frequency higher than the PTA window, and the SGWB signal is dominated by the IR tail signal, which scales as $\Omega_{\rm GW} \propto f_{\rm GW}^3$. From Eqs. (1) and (2), we obtain the asymptotic behavior of $T_{\rm dec} \propto f_a^{4/3}$ (or $m_a \propto f_a^{8/3}$), up to the log correction in Eq. (2), toward large f_a limit. We show this bound (green region) in the usual axion parameter space in the bottom-left corner of Fig. 3. The NG15 constraint on f_a values for $N_{\rm DW} = 1$ corresponds to $f_a > H_{\rm inf}/(2\pi)$. Therefore, it does not apply to cosmic strings linked to quantum fluctuations during inflation.

Note that Eqs. (1) and (2) assume a standard cosmological history, i.e., a transition between the radiation era and the matter era occurring at $T_{\rm eq} \sim 1$ eV. In the region of parameter space where the axion abundance from the string network exceeds the dark matter abundance [see Eq. (14)], the matter era starts earlier, and the cosmological evolution is not viable. The nonstandard cosmological history will

[6]Derived by solving numerically Eq. (2) with $f_{\rm GW} \simeq 20$ Hz and $h^2\Omega_{\rm GW} \simeq 10^{-8}$ for LIGO.

modify the PTA data (e.g., the calibration of pulsar timing data and the dispersion measure) and also the SMBHB modeling [130]. Ignoring its impact on PTA data, we can still estimate how the axion overabundance affects our constraint, just from the dilution effect on the GW spectrum [12,21,22]; see Eq. (B3) in Appendix B. In Fig. 3, the dot-dashed green line shows the modified PTA constraint due to the diluted GW spectrum from the axion overabundance; see Appendix B for the estimate of the scaling.

1. $\Delta N_{\rm eff}$ and dark matter constraints

Although the PTA constraint excludes a large region of the axion parameter space, there exist other theoretical bounds. Axionic strings are known to emit axion particles dominantly [31]. Depending on its mass, the axion can contribute to either dark radiation or cold dark matter. Axions that are relativistic at the time of big bang nucleosynthesis (BBN) are subject to the dark radiation bound expressed as a bound on the number of extra neutrino species, $\Delta N_{\rm eff} < 0.46$ [131]. There are uncertainties in deriving this bound linked to the log correction to the number of strings in the global-string network evolution [35–37,85]. In this paper, we quote two bounds: the one relying on the semianalytic calculation [22] by Chang and Cui (CC) and the lattice result [23] by Gorghetto *et al.* (GHN),

$$f_a \lesssim 10^{15}\ \mathrm{GeV}\left[\frac{\Delta N_{\rm eff}}{0.46}\right]^{\frac{1}{2}} \times \begin{cases} 3.5 & \text{(CC)}, \\ 0.88\left[\frac{90}{\log(\frac{f_a}{H_{\rm BBN}})}\right]^{3/2} & \text{(GHN)}, \end{cases} \tag{13}$$

where we implicitly assume $\lambda \sim 1$ for the GHN bound and $H_{\rm BBN} \simeq 4.4 \times 10^{-25}$ GeV is the Hubble parameter at BBN scale ($T_{\rm BBN} \simeq$ MeV). Since ALPs have a small mass at late times, they behave as cold dark matter (CDM). Subject to the uncertainty in simulations [23,37,82], the abundance Ω_a of axion dark matter from strings predicted by GHN sets a constraint on the axion,

$$f_a \lesssim 1.8 \times 10^{15}\ \mathrm{GeV}\sqrt{\left[\frac{\Omega_a}{0.266}\right]\left[\frac{25 \times x_{0,a}}{\xi_* \times 10}\right]\left[\frac{g_*(T_{\rm dec})}{3.5}\right]^{1/4}} \times \sqrt{\left[\frac{10^2}{\log(f_a/m_a)}\right]\left[\frac{10^{-22}\ \mathrm{eV}}{m_a}\right]^{1/2}}, \tag{14}$$

typically $\xi_* \approx 25$ and $x_{0,a} \approx 10$ [23]. Note that the collapse of the string-wall system[7] at $H \simeq m_a$ produces an axion abundance of the same order as the one from strings [36], therefore an $\mathcal{O}(1)$ correction is expected in Ω_a in Eq. (14). We show both dark radiation and dark matter bounds in Fig. 3. We see that the PTA constraint becomes competitive with the equivocal $\Delta N_{\rm eff}$ bound for $m_a \lesssim 10^{(-22,-23)}$ eV.

2. Effects of nonstandard cosmology

So far, the standard ΛCDM cosmology [131] has been assumed. On the other hand, alternative expansion histories to the usually assumed radiation era are not unlikely above the BBN scale, such as a period of matter domination or kination resulting in a strongly different spectrum of GW for cosmic strings [12,21,22,77,133]. Nonetheless, the nonstandard cosmology modifies the cosmic-string GW spectrum in the high-frequency direction. From Eq. (1), the nonstandard era must end below the MeV scale to substantially change the SGWB in the PTA window. We have checked the effects of matter and kination eras with PTArcade and found that such SGWB distortion cannot improve the global-string interpretation of PTA data. In addition, we expect only a negligible effect on the PTA bound obtained in this work.

3. QCD axion

From Fig. 3, the PTA data can exclude some parts of the QCD axion (red line). However, this region of parameter space is already excluded due to the overabundance of axion dark matter or due to $\Delta N_{\rm eff}$ bounds. To relax these bounds, one can invoke a scenario where cosmic strings decay during a matter-domination era (or any era with the equation of state smaller than that of radiation), which efficiently dilutes these relics but still allows for a GW signal in the PTA frequency range [22,24,25]. Interestingly, such matter-domination era at early times can imprint a specific signature in the SGWB from global strings, which can be observed in future-planned GW experiments at frequencies above nanohertz frequencies [12,21,22,134].

B. Result for $N_{\rm DW} > 1$, implications for heavy axions

We fit the DW SGWB, varying $\{T_\star, \alpha_\star, \beta, \delta\}$, to the PTA data. Because the posteriors of β and δ are unconstrained, we show only the 2D posterior of $\{T_\star, \alpha_\star\}$ in Fig. 2 (right). The DW SGWB can fit the PTA data in the dark blue region to 1σ. The best-fit value of $\{T_\star, \alpha_\star\}$ is translated via Eq. (7) into $m_a F_a^2 \simeq 2.6 \times 10^{15}$ GeV and corresponds to the benchmark spectrum and line in Figs. 1 and 3, respectively. However, for large enough $\alpha_\star$, the DW generates a GW signal stronger than the PTA signal, leading to a constraint in the gray region in Fig. 2 (right). The constraint is the strongest $\alpha_\star \lesssim 0.02$ at $T_\star \simeq$ 13.8 MeV when the peak of the SGWB is centered in the PTA window; see also Eq. (11). For $T_\star >$ 13.8 MeV (<13.8 MeV), the GW spectrum has its IR (UV) tail in the PTA range; thus, the constraint on $\alpha_\star$ becomes weaker.

For heavy axions with $Z_{N_{\rm DW}}$ symmetry whose mass depends on the explicit symmetry-breaking scale $\Lambda \simeq \sqrt{m_a F_a}$ where $F_a = f_a/N_{\rm DW}$, the PTA constraint in Fig. 2 (right) is translated via Eq. (7) into a bound on

[7]The collapse of the system when cosmic strings reenter the horizon also produces GWs [132] when the string (domain-wall) formation happens before (after) inflation, e.g., in the preinflationary axion scenario.

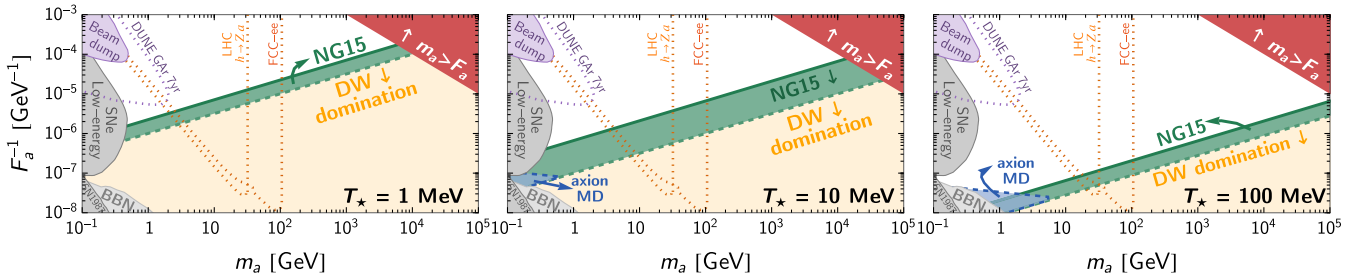

FIG. 4. The PTA-DW constraint (in green) changes with $T_\star$. For fixed $T_\star$ and m_a, the constrained range of F_a in green is derived from the $\alpha_\star$ constrained region of Fig. 2 (right), using Eq. (7). The yellow region corresponds to $\alpha_\star > 1$, which corresponds to the DW domination and can change the GW prediction; we do not extend the constraint into this region. For $T_\star \gtrsim 302$ MeV [cf. Fig. 2 (right)], NG15 data constrain $\alpha_\star > 1$; that is, the green band overlays part of the yellow region. The blue region is where the axions—produced from DW annihilations—dominate the Universe before they decay prior to BBN. In this case, the theoretical prediction for the GW spectrum also has to be reevaluated.

$\{F_a, m_a\}$ with the degeneracy among them. For a fixed $T_\star$, we obtain the excluded region on the axion parameter space, i.e., the green region of Fig. 4. Very large f_a corresponds to $\alpha_\star > 1$; the DW-domination era occurs before it decays and should affect the GW prediction. We do not extend our PTA bound in the DW-domination regime, shown in yellow in Fig. 4. In fact, Eq. (9) assumes a radiation-dominated universe. Constraining the DW-domination region requires computing the evolution of the DW network and its SGWB in a universe with a modified equation of state. We leave this nontrivial task for future investigation; see also [135]. To be conservative, we mark this region unconstrained for now, although we expect some constraints will prevail there.

Because the PTA constraint on $\alpha_\star$ is not linear in $T_\star$, the width of the PTA band is maximized only for $T_\star \simeq 13.8$ MeV where the bound on $\alpha_\star$ is the strongest. In Fig. 3, we also show the ability to constrain axion parameter space with the PTA-DW signal. We obtain the constraint by summing the excluded regions for the range MeV $\leq T_\star \lesssim$ 302 MeV, where $T_\star \simeq 302$ MeV is where the constraint has $\alpha_\star \geq 1$ in Fig. 2 (right). The upper limit of the green region (large m_a) of Fig. 3 is set by the constraint at $T_\star =$ MeV: $\alpha_\star \gtrsim 0.2$; see Fig. 2 (right). Using Eq. (7), this upper bound is defined as $m_a F_a^2 \gtrsim 2 \times 10^{11}$ GeV^3. Some regions above and within the green band (smaller $m_a F_a^2$) will be probed by future particle physics experiments [126,127,136–138].

Other than the PTA bound, the $\{T_\star, \alpha_\star\}$ parameter space is subject to theoretical constraints related to the DW decay and its by-products. In this work, we consider that the heavy axion produced from the DW decay subsequently decays into SM particles, e.g., photons via $\mathcal{L} \supset -\frac{g}{4} F\tilde{F}\theta$ with the decay rate $\Gamma_{\theta\gamma} = m_a^3 g^2/(64\pi)$ [139]. Using this to $F_a = 1.92\alpha_{\rm EM}/(2\pi g_{\theta\gamma})$, the decay is efficient when $\Gamma_{\theta\gamma} > H(T)$, which is equivalent to

$$T < T_{\theta\gamma} \equiv 236 \text{ MeV} \left[\frac{10.75}{g_*(T_{\theta\gamma})}\right]^{\frac{1}{4}} \left[\frac{m_a}{\text{GeV}}\right]^{\frac{1}{2}} \left[\frac{10^6 \text{ GeV}}{f_a/N_{\rm DW}}\right]. \quad (15)$$

The bound $T_{\rm BBN} < T_{\theta\gamma}$ is similar to the BBN bound from [140] in Figs. 3 and 4.

Moreover, the heavy axion that behaves nonrelativistically might decay after it dominates the Universe if $T_\star > T_{\rm dom} > T_{\theta\gamma}$, where the temperature $T_{\rm dom}$ corresponds to the heavy-axion domination, i.e., $\rho_a(T_{\rm dom}) = \rho_a(T_\star)(a_\star/a_{\rm dom})^3 = \rho_{\rm tot}(T_{\rm dom})$,

$$T_{\rm dom} \simeq 0.02 \text{ MeV} \left[\frac{10.75}{g_*(T)}\right]^{\frac{1}{2}} \left[\frac{50 \text{ MeV}}{T_\star}\right] \left[\frac{m_a}{\text{GeV}}\right] \left[\frac{f_a/N_{\rm DW}}{10^6 \text{ GeV}}\right]^2. \quad (16)$$

We mark this region in the blue region of Fig. 4. For the sum of PTA constraints varying $T_\star$ in Fig. 3, we omit showing the color of the axion matter-domination (MD) region, which cuts the PTA region from the low-m_a region.[8] This heavy axion induces a matter-domination era that would change the GW prediction, e.g., the causality tail of the spectrum gets distorted [141–143]. Although this spectral distortion would change the fitting of the data, it would affect the constraint derived here minimally for two reasons. First, the blue region in Fig. 4, leading to the axion-MD region, is smaller than the constrained region. Second, within this region, we find $T_{\rm dom}/T_{\theta\gamma} \lesssim 10$ which leads to $\Omega_{\rm GW} \propto f_{\rm GW}$ for frequencies in the range $[10^{-2/3}, 1] \times f_{\rm p}^{\rm DW}$, using Eq. (4.5) of [141] where $f_{\rm p}^{\rm DW}$ is the peak frequency (11).

1. Other effects

The friction from axionic DW interactions with particles of the thermal plasma could change the network's dynamics [144] and potentially the SGWB spectrum. Another effect that could change the bounds is the potential collapse of DW into primordial black holes [44,45,145–149]. Nonetheless, since the prediction is based on the spherical

[8] Using Eq. (7) with $\alpha_\star = 1$ and $T_{\theta\gamma} < T_{\rm dom}$, the cut follows $236(m_a/\text{GeV}) < (F_a/10^6 \text{ GeV})^2$.

collapse, we would need a large-scale numerical simulation of DW to check whether the primordial black hole formation can be realized. Finally, further QCD effects can impact the DW decays relevant for PTAs [135,150,151].

IV. CONCLUSION

We analyzed the consequences of the 15-yr NANOGrav data on the parameter space of postinflationary axions. The bounds in Fig. 3 come in two distinct regimes: the low- and large-axion-mass ranges, which are, respectively, associated with signals from axionic global strings ($N_{\rm DW}=1$) and domain walls ($N_{\rm DW}>1$). In the low-axion-mass region, the constraint on f_a is strongest for $m_a \ll 10^{-17}$ eV and reads $f_a < 2.8\times 10^{15}$ GeV. It is competitive with the $\Delta N_{\rm eff}$ bound. At high masses, 0.1 GeV $\lesssim m_a \lesssim 10^3$ TeV, a substantial region, corresponding to $m_a(f_a/N_{\rm DW})^2 \gtrsim 2\times 10^{11}$ GeV^3, can be excluded for DWs decaying in the $T_* \propto \sqrt{V_{\rm bias}} \sim 1$–$300$ MeV range.

This study motivates the investigation of the SGWB in the regime of DW domination, as this knowledge could lead to substantial new constraints at large m_a and f_a values. Once the network of DWs dominates the Universe, the scaling regime might be lost. DWs would instead enter the stretching regime [152] where the energy density scales as $\rho \propto a^{-1}$, the equation of state of $-2/3$ leading to the accelerated cosmic expansion could be in tension with several cosmological observations [135,153]. Moreover, a period of early DW domination together with the axion matter domination can also affect the SGWB spectra from DWs and cosmic strings [12,141–143,154,155].

To conclude, GWs are a promising tool to probe axion physics. PTA measurements have opened the possibility of observing the Universe at the MeV scale, enabling us to constrain several classes of axion models. By combining NG15 with other datasets from EPTA, InPTA, PPTA, and CPTA Collaborations, the constraints on axions can become more stringent, similar to what has been shown for other cosmological sources [156,157]. Other planned GW observatories will permit the search for different parts of the predicted SGWB from axion physics and probe the axion parameter spaces uncharted by the PTAs. Moreover, the synergy of GW experiments over a wide frequency range will allow us to distinguish the axion-GW signals from other SGWBs from astrophysical and cosmological sources [158].

ACKNOWLEDGMENTS

We are indebted to Andrea Mitridate for teaching us PTArcade and for his substantial help on the analysis. We thank Marco Gorghetto for discussions and Matthias Koschnitzke for his technical support. P. S. is funded by Generalitat Valenciana Grant No. PROMETEO/2021/083. This work is supported by the Deutsche Forschungsgemeinschaft under Germany's Excellence Strategy—EXC 2121 "Quantum Universe"—390833306 and the Maxwell computational resources operated at Deutsches Elektronen-Synchrotron (DESY), Hamburg, Germany.

APPENDIX A: PRIORS FOR ANALYSIS

Table I shows the ranges of priors for the parameters in global-string and domain-wall scenarios used for the Monte Carlo Markov chain tools. For the SMBHB signal, we use the prior of the power-law fitted spectrum, which is translated from the 2D Gaussian distribution in SMBHB parameters, motivated by the simulated SMBHB populations [7] and implemented in PTArcade. The Bayes factors reported for our two new-physics cases depend on the evidence of this SMBHB template.

APPENDIX B: AXION MATTER DOMINATION IN $N_{\rm DW}=1$ CASE

The string network with string tension $\mu = \pi f_a^2 \log(\lambda^{1/2} f_a/H)$ during the scaling regime has energy density $\rho_{\rm net} \simeq \mu/t^2 \simeq G\mu\rho_{\rm tot}$, where we omit the $\mathcal{O}(1)$ numerical factors. At $H(T_{\rm dec}) \sim m_a$, the network decays into axions (each of energy $\sim H \sim m_a$ [31,44,159,160]) with energy density $\rho_{\rm net}(T_{\rm dec})$ where $T_{\rm dec}$ in Eq. (4). They redshift as nonrelativistic particles, $\rho_{\rm net}(T) \propto a^{-3}$, and eventually dominate the SM radiation at temperature

$$T'_{\rm dom} \simeq T_{\rm dec} G\mu(T_{\rm dec}) \left[\frac{g_*(T_{\rm dec}) g_{*s}(T'_{\rm dom})}{g_*(T'_{\rm dom}) g_{*s}(T_{\rm dec})}\right], \quad \text{(B1)}$$

where we used $a^{-3} \propto g_{*s}(T)T^3$. The domination before the radiation-matter equality $T'_{\rm dom} > T_{\rm eq} \simeq 0.75$ eV leads to

TABLE I. Ranges of priors for global-string and domain-wall parameters used for the analysis.

Models	Parameters	Priors
Global strings	f_a (GeV): $U(1)$ breaking scale	Log uniform: $[10^{15}, 10^{17}]$
	$T_{\rm dec}$ (GeV): Temperature when string network decays [related to axion mass m_a via Eq. (4)]	Log uniform: $[10^{-8}, 10]$
Domain walls	$\alpha_\star$: Energy fraction in DWs at decay	Log uniform:$[10^{-2}, 1]$
	$T_\star$ (GeV): DW annihilation temperature	Log uniform: $[10^{-3}, 10]$
	δ: Width of GW spectrum	Uniform: [1, 3]
	β: Slope of GW spectrum for $f > f_{\rm p}$	Uniform: [1, 3]

dark matter overabundance. This bound is similar to Eq. (14) and the gray region denoted "DM strings" in Fig. 3. A universe with $T'_{\rm dom} > T_{\rm eq}$ cannot resemble the standard ΛCDM model. Below, we compute the modified GW spectrum from global strings due to the earlier matter era, although we do not use it for analyzing the PTA data, which rely on the standard cosmology assumption for, e.g., the calibration of pulsar timing data and the dispersion measure [130].

We set today's time as when the photon temperature matches the CMB observation. The GW signal emitted with frequency $f_{\rm GW}^{\rm emit}$ at temperature $T(a_{\rm emit})$ has the frequency today $[f_{\rm GW}^{\rm emit}(a_{\rm emit}/a_0)]$, which is the same for ΛCDM and non-ΛCDM cases, i.e., $(a_{\rm emit}/a_0) = (a_{\rm emit}/a_0)_{\Lambda\rm CDM}$. On the other hand, the emitted GW energy density $[\Omega_{\rm GW} \sim (\rho_{\rm GW}^{\rm emit}/\rho_{\rm tot,0})(a_{\rm emit}/a_0)^4]$ gets diluted as $\rho_{\rm tot,0} > \rho_{\rm tot,0}^{\Lambda\rm CDM}$ [12]. We define the dilution factor Υ as

$$\Upsilon(m_a, f_a) \equiv \frac{\Omega_{\rm GW,0}}{\Omega_{\rm GW,0}^{\Lambda\rm CDM}} = \frac{\rho_{\rm tot,0}^{\Lambda\rm CDM}}{\rho_{\rm tot,0}} \simeq 0.2 \left[\frac{g_{*s}(T'_{\rm dom})}{g_*(T'_{\rm dom})}\right] \left(\frac{10\ {\rm eV}}{T'_{\rm dom}}\right), \tag{B2}$$

which scales as $\Upsilon \propto m_a^{-1/2} f_a^{-2}$, neglecting the log correction and using Eqs. (4) and (B1). For $\Upsilon < 1$ the axion is dominating the Universe today. Because of axion overabundance, the GW spectrum in Eq. (2) becomes

$$\Omega_{\rm GW,0}(f_{\rm GW}) = \Omega_{\rm GW,0}^{\Lambda\rm CDM}(f_{\rm GW})\Upsilon(m_a, f_a) \times \mathcal{F}(f_{\rm GW}, f_{\rm GW}^{\rm dom}), \tag{B3}$$

where the shape function $\mathcal{F}$ represents the modified causality tail due to the matter domination [136] below the horizon-scale frequency at the start of matter domination, i.e., $\Omega_{\rm GW} \propto f_{\rm GW}$ for $f_{\rm GW} < f_{\rm GW}^{\rm dom} = H_{\rm dom}(a_{\rm dom}/a_0)$ instead of $\Omega_{\rm GW} \propto f_{\rm GW}^3$ during the radiation era.

Assuming the PTA data do not change with the modified cosmology, we use Eqs. (2), (4), (B1), and (B3) to estimate how the PTA constraint from global strings (the green region in the bottom-left corner of Fig. 3) is deformed due to the axion overabundance. For $m_a \lesssim 10^{-22}$ eV, the PTA constraint is compatible with standard cosmology. For $10^{-22} \lesssim m_a \lesssim 10^{-17}$ eV, the GW amplitude gets diluted by the axion overabundance. The constraint scales as $m_a \propto f_a^4$, as opposed to $f_a =$ constant when assuming a standard cosmological evolution. For $m_a \gg 10^{-17}$ eV, the IR tail is constrained by PTA. The constraint scales asymptotically as $m_a \propto f_a^2$, using the IR tail $\Omega_{\rm GW} \propto f_{\rm GW}$. We show the modified constraint as the dashed green curve in Fig. 3.

APPENDIX C: GLOBAL-STRING AND DOMAIN-WALL SIGNALS WITHOUT SMBHB BACKGROUND

In contrast with the analysis presented in the main text, which interprets the NG15 signal in terms of SMBHBs, this appendix assumes the absence of an astrophysical background and instead interprets the signal as a SGWB from global strings or domain walls. Figure 5 shows the

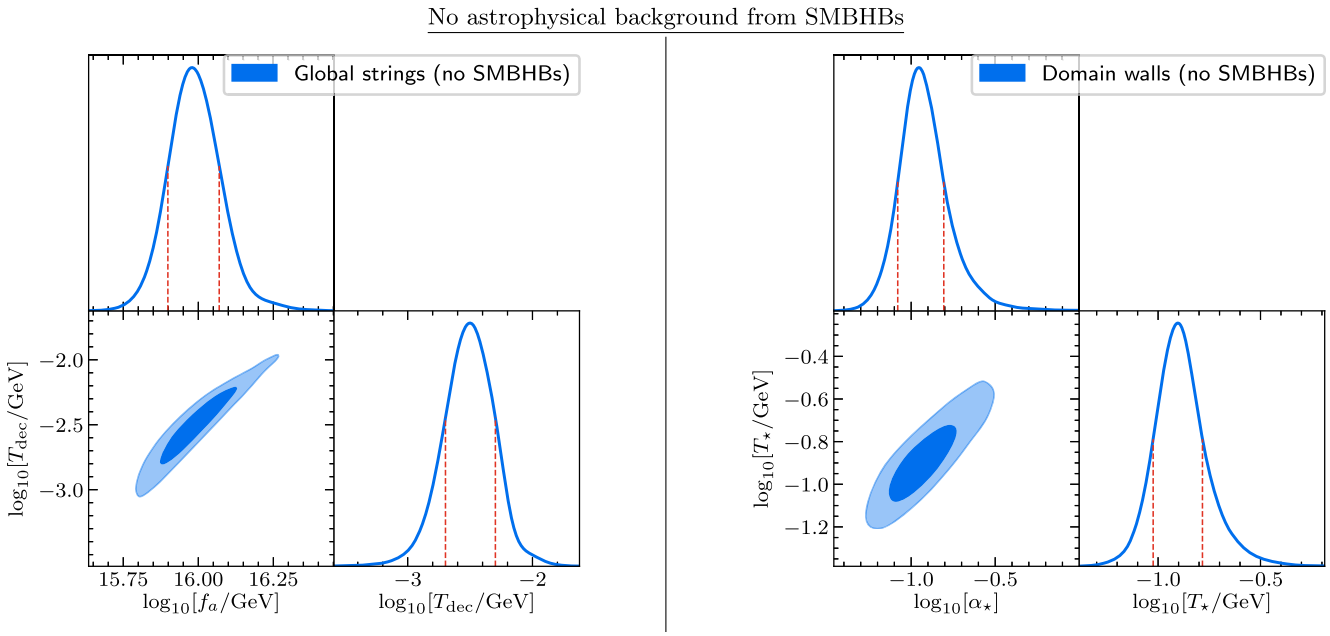

FIG. 5. Best fits to NG15 data. Left: the 2D posterior for the global-string SGWB template presented in the main text. Via Eq. (4), the best fit corresponds to axion parameters $\{f_a, m_a\} = \{9.55 \times 10^{15}\ {\rm GeV}, 3.89 \times 10^{-15}\ {\rm eV}\}$. The comparison of the fit to the SMBHB signal yields the BF $\simeq 22.8$. Right: result for domain-wall SGWB, which has the BF $\simeq 23.4$. The best-fitted axion parameters satisfy $m_a F_a^2 = 2.4 \times 10^{15}\ {\rm GeV}^3$; cf. Eq. (7). The posteriors for the UV slope β and the width δ are not constrained, as only the IR tail of the spectrum (10) lies within the PTA frequency range for the chosen range of T_*.

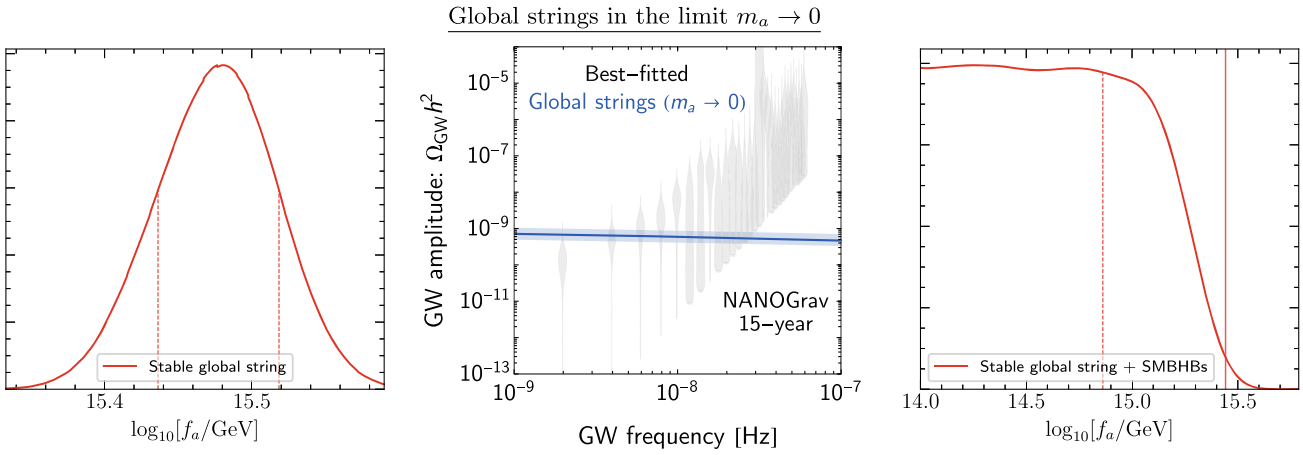

FIG. 6. Left: the 1D posterior of the stable global-string SGWB, using NG15 dataset. The best-fitted f_a value is $f_a \simeq 2.99^{+0.31}_{-0.26} \times 10^{15}$ GeV at 68% CL and the BF is 1.45×10^{-3}, for the comparison with the SMBHBs. The vertical red line indicates the 1σ region. Middle: the best-fitted GW background from stable global strings and its range within 1σ region of f_a, laying over the violins of NG15 observation. Right: the 1D posterior of the stable global-string SGWB + SMBHBs contribution, fitted to NG15 dataset. The best-fitted string scale is $f_a \simeq 1.83^{+5.45} \times 10^{15}$ GeV at 68% CL and the BF is 0.64, compared to the SMBHBs alone. The vertical dashed line locates the 1σ region, while the solid vertical line marks the K ratio $= 0.1$ and sets a limit on $f_a < 2.77 \times 10^{15}$ GeV.

two-dimensional posterior of the global-string and the domain-wall parameters. For global strings, the best-fit (maximum posterior) is at $f_a = 9.55^{+2.19}_{-1.63} \times 10^{15}$ GeV and $T_{\mathrm{dec}} = 3.16^{+1.88}_{-1.15}$ MeV at 68% CL. The central value of T_{dec} corresponds to $m_a = 3.89 \times 10^{-15}$ eV; cf. Eq. (4). For domain walls, the best fit is at $\alpha_\star = 0.111^{+0.045}_{-0.027}$ and $T_\star = 125^{+31}_{-39}$ MeV, with the error within the 68% CL region. Their central values give $m_a F_a^2 = 2.4 \times 10^{15}$ GeV^3; cf. Eq. (7). We calculate the Bayes factor (compared to the SGWB from SMBHBs) from PTArcade and find that the BFs are 22.8 for global strings and 23.4 for domain walls. When the SMBHB background is added, we find that the BF for both cases increases to 26.0 for global strings and 44.7 for domain walls. However, the values of the best-fitted parameters change only slightly: $f_a = 9.87^{+2.67}_{-2.02} \times 10^{15}$ GeV and $T_{\mathrm{dec}} = 3.50^{+2.44}_{-1.48}$ MeV, at 68% CL for global strings, corresponding to $m_a = 4.78 \times 10^{-15}$ eV. For domain walls, we have $\alpha_\star = 0.114^{+0.060}_{-0.033}$ and $T_\star = 128^{+55}_{-33}$ MeV, corresponding to $m_a F_a^2 = 2.6 \times 10^{15}$ GeV^3.

APPENDIX D: GLOBAL STRINGS FOR $m_a \to 0$

The constrained region in Fig. 2 (middle) shows that the PTA signal from global strings with small T_{dec} (or small m_a) reaches the asymptotic value of $f_a \simeq 2.8 \times 10^{15}$ GeV. This is because the cutoff specified by T_{dec} moves outside of the PTA range, and the SGWB spectrum is seen as the one from stable global strings in the limit T_{dec} or $m_a \to 0$. Figure 6 (left) shows the 1D posterior of signal from the stable global strings, which has the best-fitted spectrum at $f_a \simeq 2.99^{+0.31}_{-0.26} \times 10^{15}$ GeV at 68% CL. Nonetheless, it has the BF of 1.45×10^{-3} due to its red-tilted spectrum, poorly fitting the data, as shown in Fig. 6 (middle). When the SMBHB background is added in Fig. 6 (right), the BF becomes 0.64, meaning that the stable string spectrum worsens the fit compared to the SMBHB alone. Although the fit is not good, the constraint can be derived when the global-string SGWB becomes too strong (too large f_a) using the K ratio, discussed in the main text (see also Ref. [5]). The vertical solid line in Fig. 6 (right) shows the limit set by the NG15 data (K ratio $= 0.1$): $f_a < 2.77 \times 10^{15}$ GeV, which is similar to the bound obtained from Fig. 2 (middle) in the $T_{\mathrm{dec}} \to 0$ limit.

APPENDIX E: COMPARISON TO OTHER NEW-PHYSICS INTERPRETATIONS OF THE SIGNAL

Figure 7 summarizes confidence levels—in terms of the BF—for explaining the NG15 dataset with new-physics interpretations. We only consider the result from the analysis using the same assumption on the SMBHB background [7]. We also omit our DW result here, which is the same analysis as in [5] and yields similar BFs. Although the axion-string template fits the NG15 well, the best-fit parameter space conflicts strongly with the ΔN_{eff} and DM abundance constraints, i.e., the benchmark point of the best fit star sits deep inside the constrained region in Fig. 3.

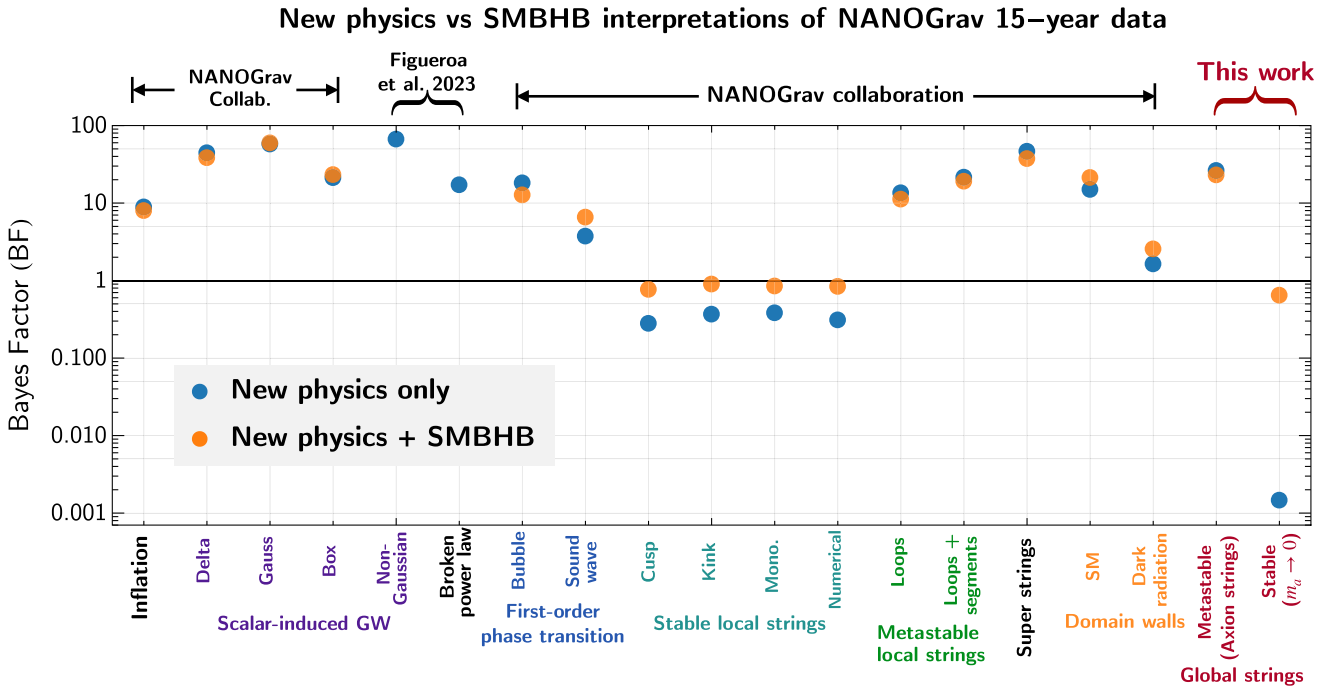

FIG. 7. Comparison of the model considered in this work and other new-physics interpretations considered by NANOGrav Collaboration [5] and Figueroa *et al.* [157]. We only consider the results using the same assumption on SMBHB background [7]. This figure extends Fig. 2 of Ref. [5].

[1] NANOGrav Collaboration, The NANOGrav 15-year data set: Evidence for a gravitational-wave background, Astrophys. J. Lett. **951**, L8 (2023).

[2] J. Antoniadis *et al.*, The second data release from the European Pulsar Timing Array III. Search for gravitational wave signals, Astron. Astrophys. **678**, A50 (2023).

[3] D. J. Reardon *et al.*, Search for an isotropic gravitational-wave background with the Parkes Pulsar Timing Array, Astrophys. J. Lett. **951**, L6 (2023).

[4] H. Xu *et al.*, Searching for the nano-hertz stochastic gravitational wave background with the Chinese Pulsar Timing Array data release I, Res. Astron. Astrophys. **23**, 075024 (2023).

[5] NANOGrav Collaboration, The NANOGrav 15-year data set: Search for signals from new physics, Astrophys. J. Lett. **951**, L11 (2023).

[6] J. Antoniadis *et al.*, The second data release from the European Pulsar Timing Array: V. Implications for massive black holes, dark matter and the early Universe, arXiv:2306.16227.

[7] NANOGrav Collaboration, The NANOGrav 15-year data set: Constraints on supermassive black hole binaries from the gravitational wave background, Astrophys. J. Lett. **952**, L37 (2023).

[8] T. W. B. Kibble, Topology of cosmic domains and strings, J. Phys. A **9**, 1387 (1976).

[9] T. W. B. Kibble, Some implications of a cosmological phase transition, Phys. Rep. **67**, 183 (1980).

[10] M. B. Hindmarsh and T. W. B. Kibble, Cosmic strings, Rep. Prog. Phys. **58**, 477 (1995).

[11] A. Vilenkin and E. P. S. Shellard, *Cosmic Strings and Other Topological Defects* (Cambridge University Press, Cambridge, England, 2000).

[12] Y. Gouttenoire, G. Servant, and P. Simakachorn, Beyond the standard models with cosmic strings, J. Cosmol. Astropart. Phys. 07 (2020) 032.

[13] P. Auclair *et al.*, Probing the gravitational wave background from cosmic strings with LISA, J. Cosmol. Astropart. Phys. 04 (2020) 034.

[14] LISA Cosmology Working Group, Cosmology with the laser interferometer space antenna, Living Rev. Relativity **26**, 5 (2023).

[15] M. Maggiore *et al.*, Science case for the Einstein telescope, J. Cosmol. Astropart. Phys. 03 (2020) 050.

[16] J. Ellis and M. Lewicki, Cosmic string interpretation of NANOGrav Pulsar Timing Data, Phys. Rev. Lett. **126**, 041304 (2021).

[17] S. Blasi, V. Brdar, and K. Schmitz, Has NANOGrav found first evidence for cosmic strings?, Phys. Rev. Lett. **126**, 041305 (2021).
[18] W. Buchmuller, V. Domcke, and K. Schmitz, From NANOGrav to LIGO with metastable cosmic strings, Phys. Lett. B **811**, 135914 (2020).
[19] R. Samanta and S. Datta, Gravitational wave complementarity and impact of NANOGrav data on gravitational leptogenesis, J. High Energy Phys. 05 (2021) 211.
[20] EPTA Collaboration, Practical approaches to analyzing PTA data: Cosmic strings with six pulsars, arXiv:2306.12234.
[21] C.-F. Chang and Y. Cui, Stochastic gravitational wave background from global cosmic strings, Phys. Dark Universe **29**, 100604 (2020).
[22] C.-F. Chang and Y. Cui, Gravitational waves from global cosmic strings and cosmic archaeology, J. High Energy Phys. 03 (2022) 114.
[23] M. Gorghetto, E. Hardy, and H. Nicolaescu, Observing invisible axions with gravitational waves, J. Cosmol. Astropart. Phys. 06 (2021) 034.
[24] N. Ramberg and L. Visinelli, Probing the early Universe with axion physics and gravitational waves, Phys. Rev. D **99**, 123513 (2019).
[25] N. Ramberg and L. Visinelli, QCD axion and gravitational waves in light of NANOGrav results, Phys. Rev. D **103**, 063031 (2021).
[26] R. D. Peccei and H. R. Quinn, *CP* conservation in the presence of instantons, Phys. Rev. Lett. **38**, 1440 (1977).
[27] R. D. Peccei and H. R. Quinn, Constraints imposed by *CP* conservation in the presence of instantons, Phys. Rev. D **16**, 1791 (1977).
[28] S. Weinberg, A new light boson?, Phys. Rev. Lett. **40**, 223 (1978).
[29] F. Wilczek, Problem of strong *P* and *T* invariance in the presence of instantons, Phys. Rev. Lett. **40**, 279 (1978).
[30] P. Sikivie, Of axions, domain walls and the early Universe, Phys. Rev. Lett. **48**, 1156 (1982).
[31] R. L. Davis, Cosmic axions from cosmic strings, Phys. Lett. B **180**, 225 (1986).
[32] R. L. Davis and E. P. S. Shellard, Do axions need inflation?, Nucl. Phys. **B324**, 167 (1989).
[33] A. Dabholkar and J. M. Quashnock, Pinning down the axion, Nucl. Phys. **B333**, 815 (1990).
[34] R. A. Battye and E. P. S. Shellard, Global string radiation, Nucl. Phys. **B423**, 260 (1994).
[35] M. Gorghetto, E. Hardy, and G. Villadoro, Axions from strings: The attractive solution, J. High Energy Phys. 07 (2018) 151.
[36] M. Gorghetto, E. Hardy, and G. Villadoro, More axions from strings, SciPost Phys. **10**, 050 (2021).
[37] M. Buschmann, J. W. Foster, A. Hook, A. Peterson, D. E. Willcox, W. Zhang, and B. R. Safdi, Dark matter from axion strings with adaptive mesh refinement, Nat. Commun. **13**, 1049 (2022).
[38] D. H. Lyth, Estimates of the cosmological axion density, Phys. Lett. B **275**, 279 (1992).
[39] M. Nagasawa and M. Kawasaki, Collapse of axionic domain wall and axion emission, Phys. Rev. D **50**, 4821 (1994).
[40] S. Chang, C. Hagmann, and P. Sikivie, Studies of the motion and decay of axion walls bounded by strings, Phys. Rev. D **59**, 023505 (1999).
[41] T. Hiramatsu, M. Kawasaki, K. Saikawa, and T. Sekiguchi, Production of dark matter axions from collapse of string-wall systems, Phys. Rev. D **85**, 105020 (2012).
[42] T. Hiramatsu, M. Kawasaki, K. Saikawa, and T. Sekiguchi, Axion cosmology with long-lived domain walls, J. Cosmol. Astropart. Phys. 01 (2013) 001.
[43] G. B. Gelmini, A. Simpson, and E. Vitagliano, Gravitational waves from axionlike particle cosmic string-wall networks, Phys. Rev. D **104**, 061301 (2021).
[44] G. B. Gelmini, A. Simpson, and E. Vitagliano, Catastrogenesis: DM, GWs, and PBHs from ALP string-wall networks, J. Cosmol. Astropart. Phys. 02 (2023) 031.
[45] G. B. Gelmini, J. Hyman, A. Simpson, and E. Vitagliano, Primordial black hole dark matter from catastrogenesis with unstable pseudo-Goldstone bosons, J. Cosmol. Astropart. Phys. 06 (2023) 055.
[46] A. Mitridate, PTArcade, 10.5281/zenodo.7876430.
[47] A. Mitridate, D. Wright, R. von Eckardstein, T. Schröder, J. Nay, K. Olum *et al.*, PTArcade, arXiv:2306.16377.
[48] R. Z. Ferreira, A. Notari, O. Pujolas, and F. Rompineve, Gravitational waves from domain walls in pulsar timing array datasets, J. Cosmol. Astropart. Phys. 02 (2023) 001.
[49] L. Bian, S. Ge, C. Li, J. Shu, and J. Zong, Domain wall network: A dual solution for gravitational waves and Hubble tension?, arXiv:2212.07871.
[50] E. Madge, E. Morgante, C. P. Ibáñez, N. Ramberg, and S. Schenk, Primordial gravitational waves in the nano-hertz regime and PTA data—towards solving the GW inverse problem, arXiv:2306.14856.
[51] K. Saikawa and S. Shirai, Primordial gravitational waves, precisely: The role of thermodynamics in the Standard Model, J. Cosmol. Astropart. Phys. 05 (2018) 035.
[52] T. S. Bunch and P. C. W. Davies, Quantum field theory in de Sitter space: Renormalization by point splitting, Proc. R. Soc. A **360**, 117 (1978).
[53] A. D. Linde, Inflation can break symmetry in SUSY, Phys. Lett. **131B**, 330 (1983).
[54] A. A. Starobinsky and J. Yokoyama, Equilibrium state of a self-interacting scalar field in the de Sitter background, Phys. Rev. D **50**, 6357 (1994).
[55] Planck Collaboration, Planck 2018 results. X. Constraints on inflation, Astron. Astrophys. **641**, A10 (2020).
[56] K. Mukaida and K. Nakayama, Dynamics of oscillating scalar field in thermal environment, J. Cosmol. Astropart. Phys. 01 (2013) 017.
[57] K. Mukaida and K. Nakayama, Dissipative effects on reheating after inflation, J. Cosmol. Astropart. Phys. 03 (2013) 002.
[58] L. Kofman, A. D. Linde, and A. A. Starobinsky, Nonthermal phase transitions after inflation, Phys. Rev. Lett. **76**, 1011 (1996).
[59] I. I. Tkachev, Phase transitions at preheating, Phys. Lett. B **376**, 35 (1996).
[60] S. Kasuya and M. Kawasaki, Can topological defects be formed during preheating?, Phys. Rev. D **56**, 7597 (1997).

[61] S. Kasuya and M. Kawasaki, Topological defects formation after inflation on lattice simulation, Phys. Rev. D **58**, 083516 (1998).
[62] I. Tkachev, S. Khlebnikov, L. Kofman, and A. D. Linde, Cosmic strings from preheating, Phys. Lett. B **440**, 262 (1998).
[63] T. W. B. Kibble, Evolution of a system of cosmic strings, Nucl. Phys. **B252**, 227 (1985).
[64] A. Albrecht and N. Turok, Evolution of cosmic strings, Phys. Rev. Lett. **54**, 1868 (1985).
[65] D. P. Bennett and F. R. Bouchet, Evidence for a scaling solution in cosmic string evolution, Phys. Rev. Lett. **60**, 257 (1988).
[66] D. P. Bennett and F. R. Bouchet, Cosmic string evolution, Phys. Rev. Lett. **63**, 2776 (1989).
[67] A. Albrecht and N. Turok, Evolution of cosmic string networks, Phys. Rev. D **40**, 973 (1989).
[68] B. Allen and E. P. S. Shellard, Cosmic string evolution: A numerical simulation, Phys. Rev. Lett. **64**, 119 (1990).
[69] C. J. A. P. Martins and E. P. S. Shellard, Extending the velocity dependent one scale string evolution model, Phys. Rev. D **65**, 043514 (2002).
[70] C. Ringeval, M. Sakellariadou, and F. Bouchet, Cosmological evolution of cosmic string loops, J. Cosmol. Astropart. Phys. 02 (2007) 023.
[71] V. Vanchurin, K. D. Olum, and A. Vilenkin, Scaling of cosmic string loops, Phys. Rev. D **74**, 063527 (2006).
[72] C. J. A. P. Martins and E. P. S. Shellard, Fractal properties and small-scale structure of cosmic string networks, Phys. Rev. D **73**, 043515 (2006).
[73] K. D. Olum and V. Vanchurin, Cosmic string loops in the expanding Universe, Phys. Rev. D **75**, 063521 (2007).
[74] J. J. Blanco-Pillado, K. D. Olum, and B. Shlaer, Large parallel cosmic string simulations: New results on loop production, Phys. Rev. D **83**, 083514 (2011).
[75] D. G. Figueroa, M. Hindmarsh, and J. Urrestilla, Exact scale-invariant background of gravitational waves from cosmic defects, Phys. Rev. Lett. **110**, 101302 (2013).
[76] C. J. A. P. Martins, I. Y. Rybak, A. Avgoustidis, and E. P. S. Shellard, Extending the velocity-dependent one-scale model for domain walls, Phys. Rev. D **93**, 043534 (2016).
[77] Y. Gouttenoire, G. Servant, and P. Simakachorn, Kination cosmology from scalar fields and gravitational-wave signatures, arXiv:2111.01150.
[78] M. Kawasaki, T. Sekiguchi, M. Yamaguchi, and J. Yokoyama, Long-term dynamics of cosmological axion strings, Prog. Theor. Exp. Phys. **2018**, 091E01 (2018).
[79] A. Vaquero, J. Redondo, and J. Stadler, Early seeds of axion miniclusters, J. Cosmol. Astropart. Phys. 04 (2019) 012.
[80] V. B. Klaer and G. D. Moore, How to simulate global cosmic strings with large string tension, J. Cosmol. Astropart. Phys. 10 (2017) 043.
[81] V. B. Klaer and G. D. Moore, Global cosmic string networks as a function of tension, J. Cosmol. Astropart. Phys. 06 (2020) 021.
[82] M. Hindmarsh, J. Lizarraga, A. Lopez-Eiguren, and J. Urrestilla, Scaling density of axion strings, Phys. Rev. Lett. **124**, 021301 (2020).
[83] D. G. Figueroa, M. Hindmarsh, J. Lizarraga, and J. Urrestilla, Irreducible background of gravitational waves from a cosmic defect network: Update and comparison of numerical techniques, Phys. Rev. D **102**, 103516 (2020).
[84] M. Buschmann, J. W. Foster, and B. R. Safdi, Early-universe simulations of the cosmological axion, Phys. Rev. Lett. **124**, 161103 (2020).
[85] M. Hindmarsh, J. Lizarraga, A. Lopez-Eiguren, and J. Urrestilla, Approach to scaling in axion string networks, Phys. Rev. D **103**, 103534 (2021).
[86] J. Baeza-Ballesteros, E. J. Copeland, D. G. Figueroa, and J. Lizarraga, Gravitational wave emission from a cosmic string loop, I: Global case, arXiv:2308.08456.
[87] M. Dine, W. Fischler, and M. Srednicki, A simple solution to the strong *CP* problem with a harmless axion, Phys. Lett. **104B**, 199 (1981).
[88] A. R. Zhitnitsky, On possible suppression of the axion hadron interactions (in Russian), Sov. J. Nucl. Phys. **31**, 260 (1980).
[89] J. E. Kim, Light pseudoscalars, particle physics and cosmology, Phys. Rep. **150**, 1 (1987).
[90] A. Vilenkin, Gravitational field of vacuum domain walls and strings, Phys. Rev. D **23**, 852 (1981).
[91] G. B. Gelmini, M. Gleiser, and E. W. Kolb, Cosmology of biased discrete symmetry breaking, Phys. Rev. D **39**, 1558 (1989).
[92] S. E. Larsson, S. Sarkar, and P. L. White, Evading the cosmological domain wall problem, Phys. Rev. D **55**, 5129 (1997).
[93] A. Vilenkin and A. E. Everett, Cosmic strings and domain walls in models with Goldstone and pseudo-Goldstone bosons, Phys. Rev. Lett. **48**, 1867 (1982).
[94] C. J. A. P. Martins and E. P. S. Shellard, Quantitative string evolution, Phys. Rev. D **54**, 2535 (1996).
[95] L. Sousa and P. P. Avelino, Stochastic gravitational wave background generated by cosmic string networks: Velocity-dependent one-scale model versus scale-invariant evolution, Phys. Rev. D **88**, 023516 (2013).
[96] L. Sousa and P. P. Avelino, Stochastic gravitational wave background generated by cosmic string networks: The small-loop regime, Phys. Rev. D **89**, 083503 (2014).
[97] J. R. C. C. C. Correia and C. J. A. P. Martins, Extending and calibrating the velocity dependent one-scale model for cosmic strings with one thousand field theory simulations, Phys. Rev. D **100**, 103517 (2019).
[98] T. Hiramatsu, M. Kawasaki, and K. Saikawa, Evolution of string-wall networks and axionic domain wall problem, J. Cosmol. Astropart. Phys. 08 (2011) 030.
[99] J. Preskill, S. P. Trivedi, F. Wilczek, and M. B. Wise, Cosmology and broken discrete symmetry, Nucl. Phys. **B363**, 207 (1991).
[100] M. Gleiser and R. Roberts, Gravitational waves from collapsing vacuum domains, Phys. Rev. Lett. **81**, 5497 (1998).
[101] T. Hiramatsu, M. Kawasaki, and K. Saikawa, Gravitational waves from collapsing domain walls, J. Cosmol. Astropart. Phys. 05 (2010) 032.
[102] M. Kawasaki and K. Saikawa, Study of gravitational radiation from cosmic domain walls, J. Cosmol. Astropart. Phys. 09 (2011) 008.

[103] T. Hiramatsu, M. Kawasaki, and K. Saikawa, On the estimation of gravitational wave spectrum from cosmic domain walls, J. Cosmol. Astropart. Phys. 02 (2014) 031.
[104] R. Zambujal Ferreira, A. Notari, O. Pujolàs, and F. Rompineve, High quality QCD axion at gravitational wave observatories, Phys. Rev. Lett. **128**, 141101 (2022).
[105] K. Saikawa, Gravitational waves from cosmic domain walls: A mini-review, J. Phys. Conf. Ser. **1586**, 012039 (2020).
[106] G. Janssen *et al.*, Gravitational wave astronomy with the SKA, Proc. Sci., AASKA14 (**2015**) 037 [arXiv:1501.00127].
[107] L. Lentati *et al.*, European Pulsar Timing Array limits on an isotropic stochastic gravitational-wave background, Mon. Not. R. Astron. Soc. **453**, 2576 (2015).
[108] G. Desvignes *et al.*, High-precision timing of 42 millisecond pulsars with the European Pulsar Timing Array, Mon. Not. R. Astron. Soc. **458**, 3341 (2016).
[109] NANOGRAV Collaboration, The NANOGrav 11-year data set: Pulsar-timing constraints on the stochastic gravitational-wave background, Astrophys. J. **859**, 47 (2018).
[110] A. Weltman *et al.*, Fundamental physics with the Square Kilometre Array, Pub. Astron. Soc. Aust. **37**, e002 (2020).
[111] LISA Collaboration, Laser interferometer space antenna, arXiv:1702.00786.
[112] K. Yagi and N. Seto, Detector configuration of DECIGO/BBO and identification of cosmological neutron-star binaries, Phys. Rev. D **83**, 044011 (2011).
[113] AEDGE Collaboration, AEDGE: Atomic experiment for dark matter and gravity exploration in space, Eur. Phys. J. Quantum Technol. **7**, 6 (2020).
[114] KAGRA, LIGO Scientific, Virgo, and VIRGO Collaborations, Prospects for observing and localizing gravitational-wave transients with Advanced LIGO, Advanced Virgo and KAGRA, Living Rev. Relativity **21**, 3 (2018).
[115] LIGO Scientific and VIRGO Collaborations, Characterization of the LIGO detectors during their sixth science run, Classical Quantum Gravity **32**, 115012 (2015).
[116] LIGO Scientific and Virgo Collaborations, Search for the isotropic stochastic background using data from advanced LIGO's second observing run, Phys. Rev. D **100**, 061101 (2019).
[117] S. Hild *et al.*, Sensitivity studies for third-generation gravitational wave observatories, Classical Quantum Gravity **28**, 094013 (2011).
[118] M. Punturo *et al.*, The Einstein telescope: A third-generation gravitational wave observatory, Classical Quantum Gravity **27**, 194002 (2010).
[119] LIGO Scientific Collaboration, Exploring the sensitivity of next generation gravitational wave detectors, Classical Quantum Gravity **34**, 044001 (2017).
[120] M. Breitbach, J. Kopp, E. Madge, T. Opferkuch, and P. Schwaller, Dark, cold, and noisy: Constraining secluded hidden sectors with gravitational waves, J. Cosmol. Astropart. Phys. 07 (2019) 007.
[121] A. Mitridate and D. Wright, PTArcade—data, 10.5281/zenodo.8102748.
[122] J. A. Ellis, M. Vallisneri, S. R. Taylor, and P. T. Baker, Enterprise: Enhanced numerical toolbox enabling a robust pulsar inference suite, Zenodo, 10.5281/zenodo.4059815 (2020).
[123] S. R. Taylor, P. T. Baker, J. S. Hazboun, J. Simon, and S. J. Vigeland, enterprise_extensions (2021), https://github.com/nanograv/enterprise_extensions.
[124] H. Jeffreys, *The Theory of Probability* (Oxford University Press, Oxford, 1998).
[125] C. O'Hare, cajohare/axionlimits: Axionlimits, https://cajohare.github.io/AxionLimits/ (2020).
[126] M. Bauer, M. Neubert, and A. Thamm, Collider probes of axion-like particles, J. High Energy Phys. 12 (2017) 044.
[127] M. Bauer, M. Heiles, M. Neubert, and A. Thamm, Axion-like particles at future colliders, Eur. Phys. J. C **79**, 74 (2019).
[128] J. E. Kim, Weak interaction singlet and strong *CP* invariance, Phys. Rev. Lett. **43**, 103 (1979).
[129] M. A. Shifman, A. I. Vainshtein, and V. I. Zakharov, Can confinement ensure natural *CP* invariance of strong interactions?, Nucl. Phys. **B166**, 493 (1980).
[130] NANOGrav Collaboration, The NANOGrav 15 yr data set: Detector characterization and noise budget, Astrophys. J. Lett. **951**, L10 (2023).
[131] Planck Collaboration, Planck 2018 results. VI. Cosmological parameters, Astron. Astrophys. **641**, A6 (2020).
[132] S. Ge, Stochastic gravitational wave background: Birth from axionic string-wall death, arXiv:2307.08185.
[133] P. Simakachorn, Charting cosmological history and new particle physics with primordial gravitational waves, Ph.D. thesis, Hamburg University, 2022.
[134] A. Ghoshal, Y. Gouttenoire, L. Heurtier, and P. Simakachorn, Primordial black hole archaeology with gravitational waves from cosmic strings, J. High Energy Phys. 08 (2023) 196.
[135] Y. Bai, T.-K. Chen, and M. Korwar, QCD-collapsed domain walls: QCD phase transition and gravitational wave spectroscopy, arXiv:2306.17160.
[136] A. Hook, S. Kumar, Z. Liu, and R. Sundrum, High quality QCD axion and the LHC, Phys. Rev. Lett. **124**, 221801 (2020).
[137] M. Bauer, M. Neubert, S. Renner, M. Schnubel, and A. Thamm, Flavor probes of axion-like particles, J. High Energy Phys. 09 (2022) 056.
[138] G. Alonso-Álvarez, J. Jaeckel, and D. D. Lopes, Tracking axion-like particles at the LHC, arXiv:2302.12262.
[139] D. Cadamuro and J. Redondo, Cosmological bounds on pseudo Nambu-Goldstone bosons, J. Cosmol. Astropart. Phys. 02 (2012) 032.
[140] P. F. Depta, M. Hufnagel, and K. Schmidt-Hoberg, Robust cosmological constraints on axion-like particles, J. Cosmol. Astropart. Phys. 05 (2020) 009.
[141] A. Hook, G. Marques-Tavares, and D. Racco, Causal gravitational waves as a probe of free streaming particles and the expansion of the Universe, J. High Energy Phys. 02 (2021) 117.
[142] D. Racco and D. Poletti, Precision cosmology with primordial GW backgrounds in presence of astrophysical foregrounds, J. Cosmol. Astropart. Phys. 04 (2023) 054.
[143] G. Franciolini, D. Racco, and F. Rompineve, Footprints of the QCD crossover on cosmological gravitational waves at pulsar timing arrays, arXiv:2306.17136.
[144] S. Blasi, A. Mariotti, A. Rase, and A. Sevrin, Axionic domain walls at pulsar timing arrays: QCD bias and particle friction, arXiv:2306.17830.

[145] T. Vachaspati, Lunar mass black holes from QCD axion cosmology, arXiv:1706.03868.
[146] F. Ferrer, E. Masso, G. Panico, O. Pujolas, and F. Rompineve, Primordial black holes from the QCD axion, Phys. Rev. Lett. **122**, 101301 (2019).
[147] A. S. Sakharov, Y. N. Eroshenko, and S. G. Rubin, Looking at the NANOGrav signal through the anthropic window of axionlike particles, Phys. Rev. D **104**, 043005 (2021).
[148] Y. Gouttenoire and E. Vitagliano, Domain wall interpretation of the PTA signal confronting black hole overproduction, arXiv:2306.17841.
[149] S.-Y. Guo, M. Khlopov, X. Liu, L. Wu, Y. Wu, and B. Zhu, Footprints of axion-like particle in pulsar timing array data and JWST observations, arXiv:2306.17022.
[150] N. Kitajima, J. Lee, K. Murai, F. Takahashi, and W. Yin, Nanohertz gravitational waves from axion domain walls coupled to QCD, arXiv:2306.17146.
[151] B.-Q. Lu and C.-W. Chiang, Nano-Hertz stochastic gravitational wave background from domain wall annihilation, arXiv:2307.00746.
[152] C. J. A. P. Martins, I. Y. Rybak, A. Avgoustidis, and E. P. S. Shellard, Stretching and Kibble scaling regimes for Hubble-damped defect networks, Phys. Rev. D **94**, 116017 (2016).
[153] A. Friedland, H. Murayama, and M. Perelstein, Domain walls as dark energy, Phys. Rev. D **67**, 043519 (2003).
[154] G. S. F. Guedes, P. P. Avelino, and L. Sousa, Signature of inflation in the stochastic gravitational wave background generated by cosmic string networks, Phys. Rev. D **98**, 123505 (2018).
[155] Y. Cui, M. Lewicki, and D. E. Morrissey, Gravitational wave bursts as harbingers of cosmic strings diluted by inflation, Phys. Rev. Lett. **125**, 211302 (2020).
[156] L. Liu, Z.-C. Chen, and Q.-G. Huang, Implications for the non-Gaussianity of curvature perturbation from pulsar timing arrays, arXiv:2307.01102.
[157] D. G. Figueroa, M. Pieroni, A. Ricciardone, and P. Simakachorn, Cosmological background interpretation of pulsar timing array data, arXiv:2307.02399.
[158] C. Caprini and D. G. Figueroa, Cosmological backgrounds of gravitational waves, Classical Quantum Gravity **35**, 163001 (2018).
[159] M. Yamaguchi, M. Kawasaki, and J. Yokoyama, Evolution of axionic strings and spectrum of axions radiated from them, Phys. Rev. Lett. **82**, 4578 (1999).
[160] T. Hiramatsu, M. Kawasaki, T. Sekiguchi, M. Yamaguchi, and J. Yokoyama, Improved estimation of radiated axions from cosmological axionic strings, Phys. Rev. D **83**, 123531 (2011).